

Temporal coherence and indistinguishability in two-photon interference effects

Anand Kumar Jha, Malcolm N. O’Sullivan, Kam Wai Clifford Chan, and Robert W. Boyd
The Institute of Optics, University of Rochester, Rochester, New York 14627, USA

(Dated: November 13, 2018)

We show that temporal two-photon interference effects involving the signal and idler photons created by parametric down-conversion can be fully characterized in terms of the variations of two length parameters—called the biphoton path-length difference and the biphoton path-asymmetry-length difference—which we construct using the six different length parameters that a general two-photon interference experiment involves. We perform an experiment in which the effects of the variations of these two parameters can be independently controlled and studied. In our experimental setup, which does not involve mixing of signal and idler photons at a beam splitter, we further report observations of Hong-Ou-Mandel- (HOM-)like effects both in coincidence and in one-photon count rates. As an important consequence, we argue that the HOM and the HOM-like effects are best described as observations of how two-photon coherence changes as a function of the biphoton path-asymmetry-length difference.

In the past few decades, much attention has been devoted to the study of two-photon interference effects involving the signal-idler pair of photons (also called biphotons) produced by parametric down-conversion (PDC) [1, 2, 3, 4, 5, 6, 7, 8, 9, 10, 11]. The Hong-Ou-Mandel (HOM) effect [2], two-photon fringes in a Franson interferometer [3, 4, 5], induced coherence without induced emission [6], frustrated two-photon creation [7], and postponed compensation [8] are some of the very interesting temporal two-photon interference effects observed among many others. All of these effects have been explained using the mathematical framework worked out by Glauber [12]. However, different conceptual pictures have often been used to describe them.

In this Rapid Communication, we construct two length parameters—the biphoton path-length difference and the biphoton path-asymmetry-length difference—in terms of the six different length parameters that a general two-photon interference experiment involves. We show that temporal two-photon interference effects, independent of the experimental setup, can be fully characterized in terms of the variations of these two parameters only. We perform an experiment in a double-pass setup in which the variations of these two parameters can be independently controlled and studied. In this setup, which does not involve mixing of signal and idler photons at a beam splitter, we further report experimental observations of “HOM-like” effects. HOM [2] and HOM-like effects [8, 9] have so far been observed only in those setups that involve mixing of signal and idler photons, arriving either simultaneously [2] or in a postponed manner [8], at a beam splitter. As an important consequence, we argue that HOM and HOM-like effects can be best understood as observations of how the degree of two-photon coherence changes as a function of the biphoton path-asymmetry-length difference defined below.

We begin by describing two-photon interference in terms of the superposition of two-photon probability amplitudes [12, 13] and represent a general two-photon two-path interference experiment by the two-photon path diagrams of Fig. 1. Diagrammatic approaches have pre-

viously also been used to describe two-photon interference effects (see Refs. [8, 9]). For conceptual clarity, we consider only the polarization-independent, temporal two-photon interference effects, assuming perfect spatial coherence. Alternatives *a* and *b* are the two pathways by which a pump photon gets down-converted and the down-converted signal and idler photons get detected at single-photon detectors D_A and D_B . Two-photon interference is observed in the coincidence count rate of detectors D_A and D_B as long as these two alternatives are coherent, i.e., indistinguishable from each other. In a two-photon interference experiment, these alternative pathways can be introduced by using beam splitters [2, 8], by passing the pump beam twice through a crystal [7], or even by using two different crystals [6]. We take the pump wave to have a Gaussian spectrum with a coherence length l_{coh}^p . We also assume that the spectral width of the pump field is much smaller than that of the signal and idler fields. In Fig. 1, the subscripts *p*, *s* and *i* stand for pump, signal, and idler, respectively; *l* denotes the optical path length traveled by a photon; and ϕ stands for phases other than the dynamical one such as phase acquired due to reflections, geometric phase [11, 14], etc. Thus l_{sa} denotes the optical path length traveled by the signal photon in alternative *a*, etc. The various path lengths and phases can

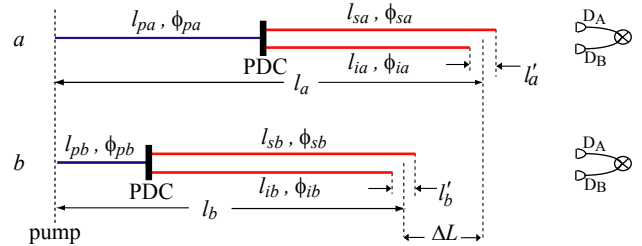


FIG. 1: (Color online) Schematic representation of two-photon interference using two-photon path diagrams. Alternatives *a* and *b* are the two pathways by which a pump photon is down-converted and the down-converted photons are detected at single-photon detectors D_A and D_B in coincidence.

be used to define two length parameters and one phase parameter as follows:

$$\begin{aligned}\Delta L &\equiv l_a - l_b = \left(\frac{l_{sa} + l_{ia}}{2} + l_{pa} \right) - \left(\frac{l_{sb} + l_{ib}}{2} + l_{pb} \right), \\ \Delta L' &\equiv l'_a - l'_b = (l_{sa} - l_{ia}) - (l_{sb} - l_{ib}), \\ \Delta\phi &\equiv (\phi_{sa} + \phi_{ia} + \phi_{pa}) - (\phi_{sb} + \phi_{ib} + \phi_{pb}).\end{aligned}\quad (1)$$

Here $l_{a(b)}$ and $l'_{a(b)}$ are the biphoton path length and the biphoton path-asymmetry length for alternative $a(b)$. In a particular alternative, the biphoton path length is defined to be the mean of the optical path lengths traveled by the signal and idler photons added to the optical path length traveled by the pump photon. The biphoton path-asymmetry length is defined to be the difference of the optical path lengths traveled by the signal and idler photons. ΔL is the difference of the biphoton path lengths l_a and l_b whereas $\Delta L'$ is the difference of the biphoton path-asymmetry lengths l'_a and l'_b . Notice that, if either ΔL or $\Delta L'$ is too large, alternatives a and b will become distinguishable and will no longer interfere.

To quantify this point, we calculate the coincidence count rate R_{AB} for detectors D_A and D_B in terms of ΔL and $\Delta L'$. The detailed calculations will be presented elsewhere. However, it can be shown by generalizing the calculations of Refs. [15, 16] that

$$R_{AB} = C[1 + \gamma(\Delta L)\gamma'(\Delta L') \cos(k_0\Delta L + k_d\Delta L' + \Delta\phi)].\quad (2)$$

Here C is a constant, k_0 is the mean vacuum wave-vector magnitude of the pump wave while $k_d \equiv (k_{s0} - k_{i0})/2$, where k_{s0} and k_{i0} are the mean vacuum wave-vector magnitudes of the signal and idler fields. $\gamma(\Delta L)$ and $\gamma'(\Delta L')$ are the normalized correlation functions of the pump and the signal-idler fields, respectively. The product $\gamma'(\Delta L')\gamma(\Delta L)$ is the degree of two-photon coherence. In the rest of this Rapid Communication, we consider only degenerate PDC in which case $k_d = 0$. Also, for simplicity, we consider only type I phase matching and assume that the signal-idler field has a Gaussian spectrum with a coherence length l_{coh} . Thus we have $\gamma(\Delta L) = \exp[-\frac{1}{2}(\Delta L/l_{\text{coh}}^p)^2]$ and $\gamma'(\Delta L') = \exp[-\frac{1}{2}(\Delta L'/l_{\text{coh}})^2]$. The general form of Eq. (2) remains the same even for other phase matching conditions. However, for other phase matching conditions, the functional form of $\gamma'(\Delta L')$ may not remain Gaussian or it may not even remain centered at $\Delta L' = 0$ [13].

We now look at the effects of varying ΔL and $\Delta L'$ on the coincidence count rate R_{AB} of Eq. (2) by considering two limiting cases.

Case I. For $\Delta L' = 0$ and $\Delta\phi = 0$,

$$R_{AB} = C [1 + \gamma(\Delta L) \cos(k_0\Delta L)].\quad (3)$$

Interference is observed in the coincidence count rate as ΔL is varied and gets washed out once ΔL exceeds the pump coherence length. Thus ΔL plays the same role in

two-photon interference as does the optical path-length difference in one-photon interference. It is because of this analogy that we call ΔL the biphoton path-length difference. The coincidence fringes seen in Franson-type interferometers [4, 5] and in the double-pass setup [7] are examples of effects due to variations in ΔL .

Case II. For ΔL and $\Delta\phi$ fixed,

$$R_{AB} = C [1 + K\gamma'(\Delta L')],\quad (4)$$

where $K = \gamma(\Delta L) \cos(k_0\Delta L + \Delta\phi)$ is constant. The coincidence count rate can show a dip when the two alternatives interfere destructively ($K < 0$), and a hump when the two alternatives interfere constructively ($K > 0$), as $\Delta L'$ is varied. These profiles, with widths equal to l_{coh} , represent how the coherence between two biphoton alternatives changes with a variation in $\Delta L'$. $\Delta L'$ has no one-photon counterpart. Effects observed in the HOM experiment [2] and in the postponed compensation experiment [8] are examples of two-photon interference effects due to variations in $\Delta L'$. In the HOM experiment [2], the effect was seen with $\Delta L = 0$, whereas in the postponed compensation experiment [8], the effects were seen in the limit $l_{\text{coh}} \ll \Delta L \ll l_{\text{coh}}^p$.

In the HOM experiment the signal and idler photons from the PDC are mixed at a beam splitter. Both photons, in the balanced position of the setup, always leave through the same output port of the beam splitter. As a result, a null is observed in the coincidence count rate at the balanced position, leading to a dip in the coincidence count rate as a function of the beam splitter position. An intuitive explanation of this effect can be given in terms of the bunching of signal and idler photons at a beam splitter [17]. However, the bunching interpretation is not adequate for the postponed compensation [8] and related experiments [9] in which HOM-like effects are observed,

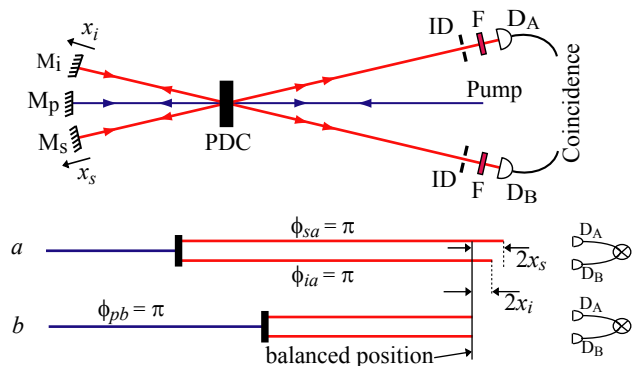


FIG. 2: (Color online) Schematic of the experimental setup and the corresponding two-photon path diagrams. In alternative a , the pump photon gets down-converted in the forward pass while in alternative b , it gets down-converted in the backward pass. F is an interference filter with 10 nm bandwidth, centered at 727.6 nm; ID is an iris diaphragm.

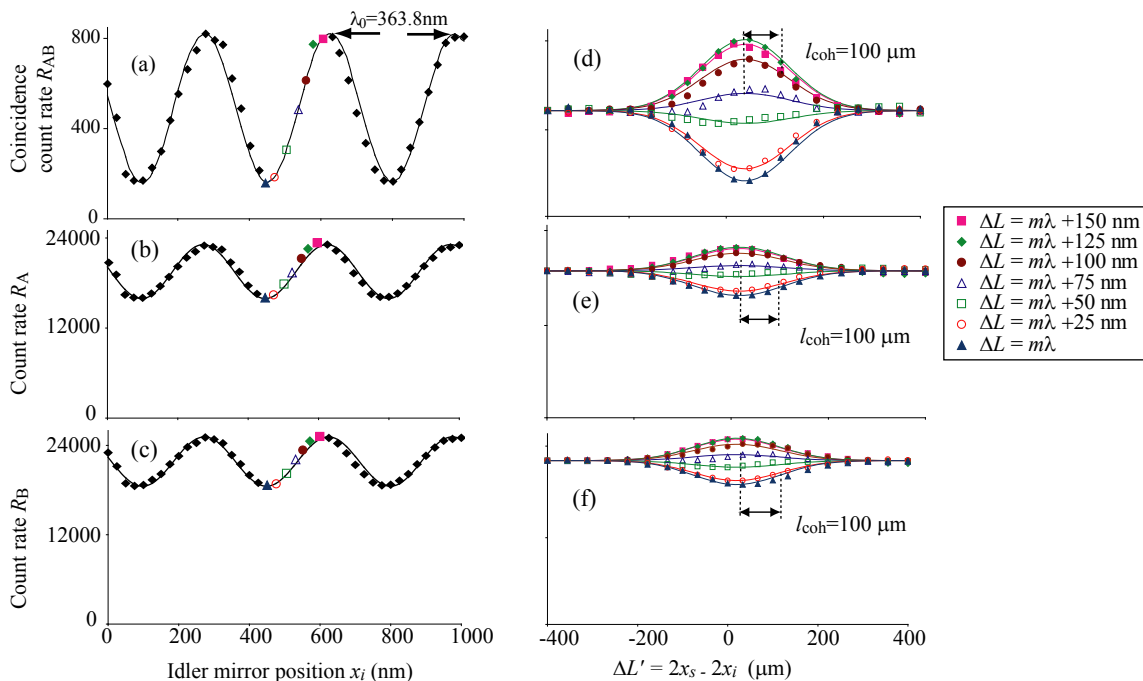


FIG. 3: (Color online) Measured (a) coincidence count rate R_{AB} , (b) count rate R_A , and (c) count rate R_B as a function of the idler mirror position. Measured (d) coincidence count rate R_{AB} , (e) count rate R_A , and (f) count rate R_B , as a function of $\Delta L'$ for various fixed values of ΔL . Solid lines are the theoretical best fits.

even when signal and idler photons do not simultaneously arrive at a beam splitter. As discussed above, both HOM and HOM-like effects are consequences of how two-photon coherence changes as a function of the biphoton path-asymmetry-length difference $\Delta L'$.

All these experiments required mixing of signal and idler photons at a beam splitter. In contrast, we next report our experimental observations of changes in two-photon coherence as a function of $\Delta L'$, in a double-pass setup (shown in Fig. 2), which does not involve mixing of signal and idler photons at a beam splitter. A similar setup was used earlier to demonstrate frustrated two-photon creation [7]. In this setup, there are many ways in which ΔL and $\Delta L'$ could be varied either independently or simultaneously, by displacing the signal (M_s), idler (M_i), and pump (M_p) mirrors. In our experiments we change only the signal and idler mirror positions.

In the balanced position of the setup of Fig. 2, the distances of the signal, idler, and pump mirrors from the crystal remain equal. We denote the displacements of the signal and idler mirrors from the balanced position by x_s and x_i , respectively. Using the two-photon path diagrams (lower part of Fig. 2), we find that $\Delta L = x_s + x_i$, $\Delta L' = 2x_s - 2x_i$, and $\Delta\phi = \pi$. Assuming ΔL to be always much smaller than the pump coherence length l_{coh}^p , which in our experiment is about 5 cm, we calculate the coincidence count rate R_{AB} for detectors D_A and D_B using Eq. (2) as

$$R_{AB} = C \{ 1 - \gamma'(2x_s - 2x_i) \cos[k_0(x_s + x_i)] \}. \quad (5)$$

A displacement of either the signal or idler mirror changes both ΔL and $\Delta L'$; therefore the coincidence count rate R_{AB} will show fringes as a function of the idler mirror position. However, equal displacements of the signal and idler mirrors in opposite directions change $\Delta L'$ while keeping $\Delta L (= x_s + x_i)$ fixed; and therefore, the coincidence count rate R_{AB} will show either a dip or a hump as a function of the joint displacement, depending on the fixed value of ΔL .

Figure 3 shows the results of our experimental investigations. A cw Ar-ion laser operating at $\lambda_0 = 363.8 \text{ nm}$ was used as a pump to produce degenerate type-I PDC. The signal and idler photons were collected into multi-mode fibers and detected using two avalanche photodiodes. The distance between the crystal and each detector was about 1.2 m. With the diaphragms set to a size of about 1.2 mm, the effective bandwidth of the signal-idler field becomes 0.85 nm, resulting in a coherence length l_{coh} of about 100 μm .

The idler mirror was first scanned around the balanced position and as a result fringes were observed in the coincidence count rate R_{AB} [Fig. 3(a)]. Next, the idler mirror was placed at different fixed positions corresponding to different values of ΔL , as shown in Fig. 3(a) and in the inset, where m is an integer. Starting from each idler mirror position, the signal and idler mirrors were displaced equally in opposite directions. Dip and hump profiles of width 100 μm were observed in the coincidence count rate R_{AB} [Fig. 3(d)].

In addition, profiles similar to that of the coincidence count rate were also observed in the single photon count rates R_A and R_B . As a function of the idler mirror position, fringes were observed in the count rates of R_A [Fig. 3(b)] and R_B [Fig. 3(c)]; and as a function of the simultaneous displacements of the signal and idler mirrors, dip and hump profiles of width $100 \mu\text{m}$ were observed in the count rates R_A [Fig. 3(e)] and R_B [Fig. 3(f)].

These one-photon effects cannot be described by second-order (in the field) coherence theory [18], because the one-photon path-length differences involved in these experiments are much longer than the coherence lengths of the one-photon fields. Interference effects in one-photon count rates have previously also been observed in many two-photon experiments including induced coherence [6], frustrated two-photon creation [7], and interference experiment from separate pulses [10]. Although these one-photon effects have been interpreted differently, they can all be described entirely in terms of the sum of two-photon interference profiles. Thus, we represent the one-photon count rate R_X at a detection position X as the sum of the coincidence count rates R_{XY_i} between X and all the other positions Y_i to which the twin of the photon detected at X can go, i.e.,

$$R_X = \sum_i R_{XY_i}. \quad (6)$$

Summing over the detector positions R_{Y_i} in Eq. (6) is the same as taking the partial trace over all the possible modes of the twin. The summation turns into an integral whenever the twin has finite probabilities of arriving at a continuous set of detection points.

Now, for the setup in Fig. 2, the twin of a photon detected at D_A can go only to D_B , and vice versa. Therefore, using Eq. (6) we find that the one-photon count rates R_A and R_B are each equal to the coincidence count rate R_{AB} . Hence, as a function of either ΔL or $\Delta L'$, the one-photon count rates show profiles similar to that of the coincidence count rate.

The dip-hump visibilities for R_{AB} , R_A and R_B were found to be 67%, 18%, and 15%, respectively. The overall interference visibilities are low due to imperfect mode

matching of the fields in the two alternatives. The visibilities of one-photon count rates are much smaller than that of the coincidence count rate, because of the limited detection efficiency of the system, which affects the one-photon count rate more strongly than the coincidence count rate. The less than perfect experimental fits are due to the uncontrollable drifts of translation stages.

We see that both in this experiment and in the HOM [2] and HOM-like [8, 9] experiments the same effect, that is, the change in two-photon coherence as a function of the biphoton path-asymmetry-length difference, is observed. However, in our experiment—in contrast to the earlier experiments—this effect is observed in a setup that does not involve mixing of signal and idler photons at a beam splitter. Moreover, to the best of our knowledge, we have observed for the first time that the changes in two-photon coherence can manifest themselves in the count rates of individual detectors as dip and hump profiles.

In conclusion, we have constructed two length parameters to describe two-photon interference involving the biphotons created by PDC. We have shown that temporal two-photon coherence depends only on these two parameters and that two-photon interference effects, including one-photon interference effects observed in certain two-photon experiments, can be fully characterized in terms of these two parameters. We have performed an experiment in which the variation of these two parameters could be independently controlled and studied. We have further reported experimental observations of HOM-like effects both in coincidence and in one-photon count rates, and we have argued that HOM and HOM-like effects can be best understood as observations of how two-photon coherence changes with a variation in the biphoton path-asymmetry-length difference.

We gratefully acknowledge financial support through a MURI grant from the U.S. Army Research Office and through an STTR grant from the U.S. Air Force Office of Scientific Research. We thank Mark Gruneisen for useful discussions. K.W.C. acknowledges the support of the Croucher Foundation.

-
- [1] L. Mandel, *Rev. Mod. Phys.* **71**, S274 (1999),
[2] C. K. Hong et al., *Phys. Rev. Lett.* **59**, 2044 (1987),
[3] J. D. Franson, *Phys. Rev. Lett.* **62**, 2205 (1989),
[4] P. G. Kwiat et al., *Phys. Rev. A* **47**, R2472 (1993),
[5] J. Brendel et al., *Phys. Rev. Lett.* **66**, 1142 (1991),
[6] X. Y. Zou et al., *Phys. Rev. Lett.* **67**, 318 (1991),
[7] T. J. Herzog et al., *Phys. Rev. Lett.* **72**, 629 (1994),
[8] T. B. Pittman et al., *Phys. Rev. Lett.* **77**, 1917 (1996),
[9] D. V. Strekalov et al., *Phys. Rev. A* **57**, 567 (1998),
[10] Y. Kim et al., *Phys. Rev. A* **61**, 051803(R) (2000),
[11] J. Brendel et al., *Phys. Rev. A* **52**, 2551 (1995),
[12] R. J. Glauber, *Phys. Rev.* **130**, 2529 (1963),
[13] M. H. Rubin et al., *Phys. Rev. A* **50**, 5122 (1994),
[14] R. Bhandari et al., *Phys. Rev. Lett.* **60**, 1211 (1988),
[15] Z. Y. Ou et al., *Phys. Rev. A* **40**, 1428 (1989),
[16] L. J. Wang et al., *Phys. Rev. A* **44**, 4614 (1991),
[17] P. Grangier, *Nature* **419**, 477 (2002),
[18] M. Born and E. Wolf (1980), *Principle of Optics*, 6th edn. (Pergamon Press, Oxford).